Brazilian Journal
of Chemical
Engineering

ISSN 0104-6632
Printed in Brazil
www.abeq.org.br/bjche

Vol. 23, No. 03, pp. 417 - 425, July - September, 2006

MODELING AND SIMULATION OF RAPID EXPANSION OF SUPERCRITICAL SOLUTIONS

M. L. Corazza[1*], L. Cardozo Filho[2] and C. Dariva[1]

[1]Departamento de Ciências Agrárias, Curso de Engenharia de Alimentos, URI,
Campus de Erechim, Av. Sete de Setembro, 1621, CEP 99700-000, Erechim - RS, Brazil.
E-mail: mlcorazza@uricer.edu.br
[2]Departamento de Engenharia Química, Universidade Estadual de Maringá,
Av. Colombo 5790, BL D-90, CEP 87020-900, Maringá - Pr, Brazil.

(Received: October 20, 2004 : Accepted: April 18, 2006)

Abstract - Rapid expansion of supercritical solution (RESS) is a promising technique for microparticle production. The literature points out that the RESS technique can be applied to process a wide range of materials including ceramics, polymers, biopolymers, pharmaceutics, and organic compounds. In order to achieve an adequate understanding of the RESS process, it is necessary to conduct more comprehensive studies involving the hydrodynamic modeling of the fluid flow through the capillary, the phase behavior of a expanding mixture, and also with regard to the microparticle formation mechanism. In this context, this work is focused on the analysis of process hydrodynamic modeling and on phase equilibrium modeling (thermodynamic modeling of supersaturation), with a phase stability test coupled. The Gibbs tangent plane distance for the phase stability test was minimized using the simulated annealing algorithm. The results showed that the thermodynamic variables exert a remarkable effect simulated variables (temperature, velocity, density and degree of supersaturation) for the profile.
Keywords: RESS process; Supersaturation; Stability analysis; Microparticle.

INTRODUCTION

Rapid expansion of supercritical solution (RESS) has been pointed to as a promising technique for micro and nanoparticle processing (Arai et al., 2002; Jung and Perrut, 2001). In a typical RESS process, a supercritical solution is expanded through a capillary (or nozzle) until reaching ambient conditions. The solvent power decreases very fast during the expansion, and as a consequence, the solute precipitates in a uniform mode. The literature on experimental work that employed RESS to process a wide range of materials, such as polymers, biopolymers, pharmaceuticals, and organic and inorganic materials is vast (Beckman, 2004; Ribeiro dos Santos et al., 2002; Jung and Perrut, 2001).

Some works focusing on fundamental aspects of the RESS process, like modeling the solution flow, nucleation, segregation, and growth phase, can also be found (Domingo et al., 1999; Turk, 1999; Helfgen et al., 2000, 2001, 2002; Turk et al., 2002; Weber et al., 2002). Unfortunately, the theoretical results obtained from these studies did not match the experimental results on the size and size distribution of the precipitated material. In this work, the hydrodynamic modeling of the RESS process uses with a consistent thermodynamic approach, where a stability analysis is conducted for the phase equilibrium problem.

MATERIAL AND METHODS

Hydrodynamic Modeling

In the literature a compressible fluid flowing with friction in a one-dimensional direction (capillary length direction) is usually used to model the RESS

*To whom correspondence should be addressed

process. Due to the low solute solubility in the supercritical solvent (solid molar fraction around $1x10^{-3}$), a pure solvent flow is also adopted. Thus, the RESS process can be described by a differential-algebraic system of equations, composed of mass, momentum, and energy balances (Eqs. 1 to 3) and by an equation of state (EOS) to account for the nonidealities in the expansion medium (Lele and Shine, 1992 e Ksibi and Subra, 1995). In this work, the Bender EOS (Platzer and Maurer, 1993) was selected due to its good performance in representing carbon dioxide thermal properties (Cp and Cv).

$$\rho\frac{dv}{dx}+v\frac{d\rho}{dx}+\frac{\rho v}{A}\frac{dA}{dx}=0 \quad (1)$$

$$\rho v\frac{dv}{dx}+\frac{dP}{dx}=-2f\frac{v^2\rho}{D} \quad (2)$$

$$\rho\frac{dh}{dx}-\frac{dP}{dx}=2f\frac{v^2\rho}{D}+\frac{\rho}{\dot{m}}\frac{dq}{dx} \quad (3)$$

where ρ is the fluid density, v is the flow velocity, P is the pressure, A is the area cross-sectional, D is the constant area section diameter, f is the Fanny friction factor, $\dot{m}$ is the mass flow, q is the heat flow, and x is the axial position.

The RESS simulation was conducted in the geometric domain presented in Figure 1, where three distinct regions can be identified: the capillary inlet (L_I), the capillary (L_{II}) (constant area region) and the free jet region (L_{III}). In the inlet region an isentropic flow was assumed; in the constant area region an adiabatic flow was adopted, and in the free jet region a isentropic flow with thermal exchange with the medium was assumed. The LIMEX code (Ehrig et al., 1999) was employed to solve the differential-algebraic system of equations. The initial velocity of the fluid was unknown, being determined iteratively by considering the maximum flow developed at the capillary end, i.e., sonic velocity at the capillary end (Helfgen et al., 2000). The Mach cone dimension was calculated employing the empirical Equations 4 and 5 (Helfgen et al., 2000).

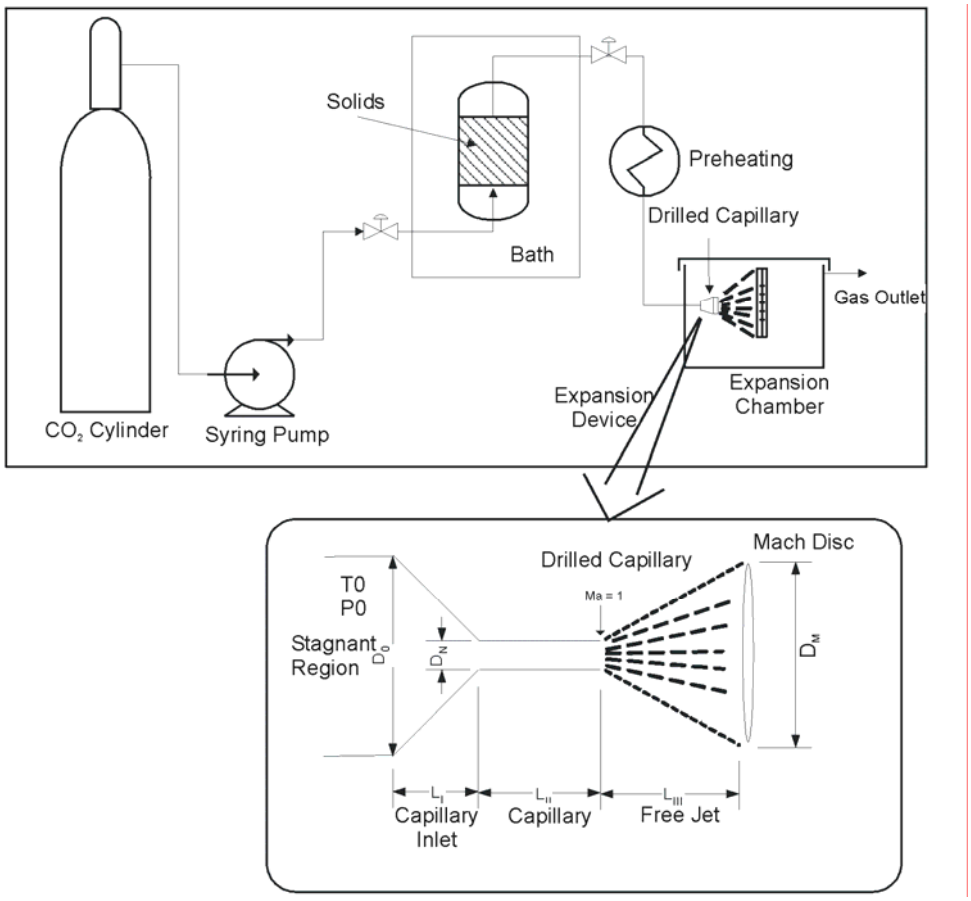

Figure 1: Schematic diagram of the RESS process for a convergent-divergent capillary.

$$L_{III} = 0.67D\sqrt{P_0/P_{CE}} \quad (4)$$

$$D_M = 0.5625L_{III} \quad (5)$$

where L_{III} and D_M are the cone length and diameter in the free jet region, respectively. P_0 and P_{ch} are the inlet and expansion chamber pressures, respectively.

The supersaturation (S) in the RESS process is a measure of the phase saturation level, and the supersaturation level can be considered the potential to formation of a new phase in the system. According to Türk (1999), the supersaturation can be calculated by Equation 6.

$$S = \frac{y_E(T_E, P_E)}{y(T,P)} \frac{\hat{\phi}(T,P,y_E)}{\hat{\phi}(T,P,y)} \quad (6)$$

where T_E and P_E are the extraction temperature and pressure, respectively (Figure 1) and $\hat{\phi}$ is the solute fugacity coefficient in the mixture related to temperature (T), pressure (P), and solute molar fraction in a particular position of the flow (y) or under extraction conditions (y_E).

The fluid residence time in the three capillary regions was evaluated as follows:

$$tR = \sum_{k=1}^{M} tR_k = z_k \overline{v}_k \quad (7)$$

where z_k is the k^{th} point in the grid solution and $\overline{v}_k$ is the average velocity of the flow between two points of the grid. M is the total number of discretizated points where the model is solved (grid).

Phase Equilibrium Calculations and Stability Test

In order to calculate the supersaturation (S), the phase equilibrium problem was solved at system temperature (T) and pressure (P) for each specific position (*x*) in the grid (balance equations). The solid phase was considered pure and referenced to a supercooled liquid state (Corazza et al., 2004a; Diefenbacher and Turk, 2002). The Soave-Redlich-Kwong equation of state (SRK-EOS) with van der Waals quadratic mixing rules was employed for phase equilibrium calculations (isofugacity conditions – Equation 8), in accordance with Corazza et al. (2004a).

$$f_{i0}^S - \hat{f}_i^F = 0 \quad (i = 1,..., \text{solute number}) \quad (8)$$

where f_{i0}^S and $\hat{f}_i^F$ are the pure solid phase and fluid phase fugacities for the "i" component, respectively. The superscript F refers to fluid phase, which can be a liquid or vapor, depending on the system condition.

A stability test was coupled with the equilibrium calculation, which requires minimization of the Gibbs tangent plane distance (TPD) (Equation 9) (Corazza et al., 2004a; Baker et al., 1982).

$$TPD = \sum_{i=1}^{N-1} y_i \left[\ln(\phi_i y_i) - \ln(\phi_i^0 y_i^0) \right] \quad (9)$$

where y_i and $\hat{\phi}_i$ are the composition and fugacity coefficient of the tried phase, and y_i^0 and $\hat{\phi}_i^0$ are the composition and fugacity coefficient of the tested phase (Corazza et al, 2004a, Hua et al., 1998; McDonald and Floudas, 1995; Michelsen, 1982). The simulated annealing (SA) algorithm, presented by Press et al. (1992), was used for Equation 9 minimization as a function of y_i (i = 1,...,N-1), where y_i is the "i" component molar composition and N is the number of components in the mixture.

RESULTS

Flow Simulation

The RESS process simulations were performed using typical dimensions for the expansion capillary: L_I = 100μm, L_{II} = 800 μm and DN = 40μm. The chamber expansion temperature and pressure, T_{ch} and P_{ch}, were kept at 298.15 K and 1.01325 bar, respectively. Following Helfgen et al. (2000), the thermal exchange coefficient in the expansion chamber, h, was fixed at 1.0×10^7 W/(m.s). The pressure at the inlet capillary, P_0, was maintained at 200 bar, while the temperature T_0 was varied in the range of 305 K to 415 K.

Figure 2 presents the simulation results on chocked mass flow (pure carbon dioxide) as a function of preexpansion temperature (T_0) along with the experimental results of Ksibi and Subra (1995). In this figure, the results with different values of friction coefficient is also depicted. It can be observed that the hydrodynamic model employed to simulate the RESS process is able to represent the mass flow experimental values as a function of preexpansion temperature. It should also be observed that more consistent values were found for a friction factor of 0.005 than for one of 0.0125 or calculating *f* by an empirical equation (Reid et al., 1988).

In Figure 3 the residence time (tR) in capillary regions I and II, related to preexpansion temperature and friction factor, *f*, is presented. A maximum residence time as a function of preexpansion temperature can be observed for the three friction factor neither of the values. It should be noted that parameters, preexpansion temperature nor friction factor, had a remarkable effect on residence time: values typical of $2.0 \pm 0.5 \times 10^{-4}$ s were observed.

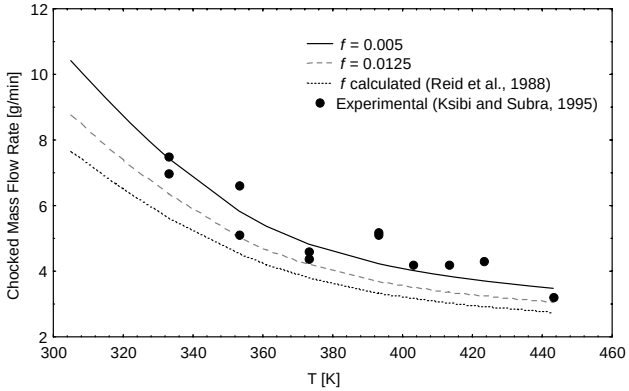

Figure 2: Chocked mass flow of pure carbon dioxide as a function of preexpansion temperature and friction factor.

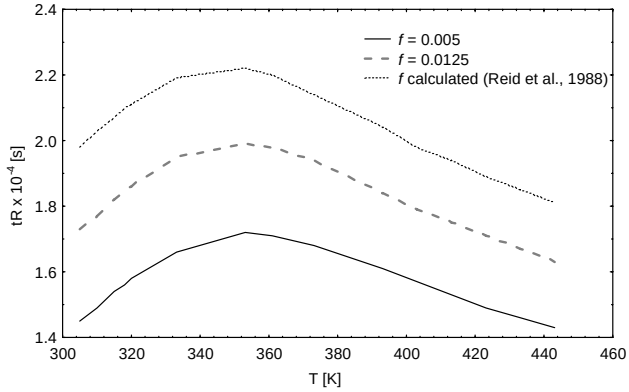

Figure 3: Residence time at the capillary inlet and in the capillary regions (regions I and II in Figure 1) as a function of preexpansion temperature and friction factor.

Additional simulations were performed using the following capillary dimensions, L_I = 330 μm, L_{II} = 350 μm and DN = 25 μm, and a expansion chamber temperature, Tch = 298.15 K, and a expansion pressure, Pch = 1.01325 bar, thermal exchange coefficient in the expansion chamber was used h = $1x10^7$ W/(m.s), and friction factor was f = 0.005. Three different initial conditions were selected: Simulation 1 P_0 = 200 bar and T_0 = 380 K; Simulation 2 P_0 = 150 bar and T_0 = 330K; and Simulation 3 P_0 = 280 bar e T_0 = 340K. In Figure 4 the profiles of temperature, T(z), velocity; v(z), density, ρ(z); Mach number, Ma(z), trough the expansion path are presented for the three simulations. In this figure $z = x/(L_I + L_{II})$ is the dimensionless position coordinate. The results presented in Figure 4 are in agreement with those under similar conditions presented by Helfgen (2000).

In general it should be noted in Figure 4 that the initial conditions exerted an effect on the profile of process variables and that a remarkable change in temperature and pressure took place in the free jet region (L_{III}). This aspect suggests that formation of a solid phase should be more pronounced in the free jet region than inside the capillary. Thus, the postexpansion conditions (expansion chamber) could be of primary importance for the characteristics of precipitated material.

In order to connect the stability test to the RESS process, the iteration values of temperature and pressure and also an overall mixture composition were used to conduct the stability analysis at each grid point in solving the hydrodynamic model. In this way, the condition for a new phase formation was tested. The binary interaction parameters of the It was considered the CO_2(1)+naphthalene(2) binary system (model system) (SRK-EOS) were taken from Corazza et al. (2004b). In Figure 5 the PT diagram is presented where the curves in the expansion path (capillary), the PT curves of SVL transitions for the binary system (SRK-EOS model), and also the vapor pressure curve for pure carbon dioxide are depicted.

It can be observed in this figure that the expansion path is dependent on the preexpansion conditions, mainly in the expansion regions inside the capillary. The expansion path progresses towards the carbon dioxide vapor pressure curve, where under that condition the solid solubility in the solution is very low. In order to check these aspects, an analysis of supersaturation of the system during expansion of the supercritical solution is conducted in the next section.

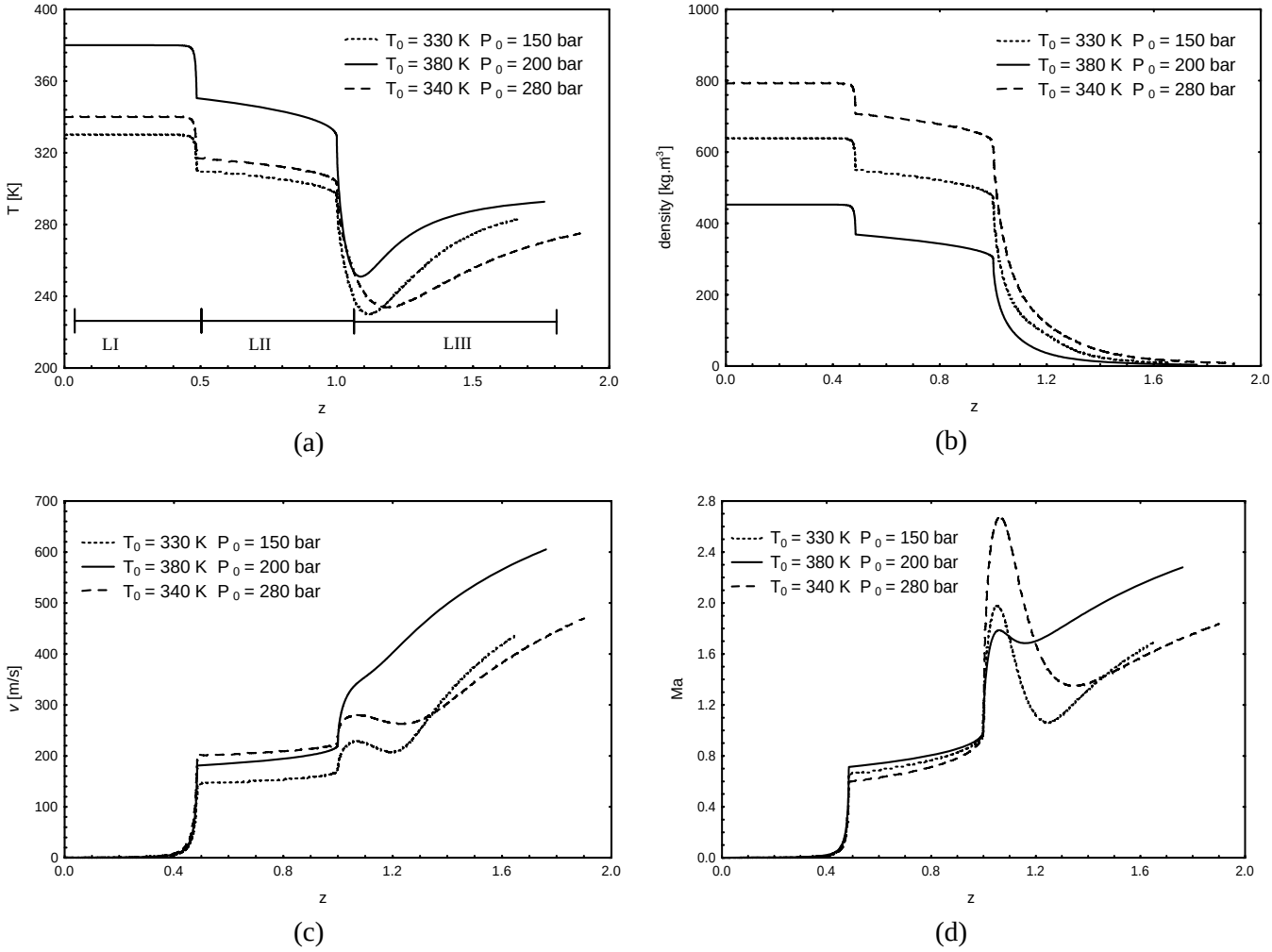

Figure 4: Temperature (a), density (b), velocity (c), and Mach number (Ma) (d) profiles for the three simulated conditions in the RESS process.

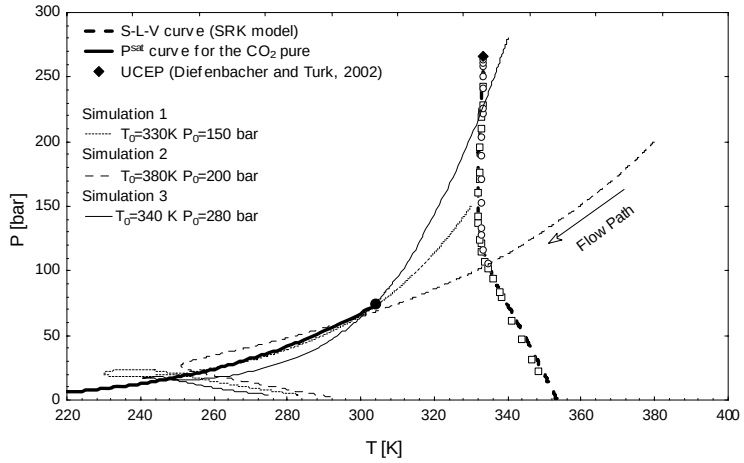

Figure 5: PT profile for RESS in the capillary regions (I and II) for a SVL equilibrium diagram of the carbon dioxide(1)+naphthalene(2) system.

Supersaturation Simulation

In order to perform the supersaturation analysis, at a given temperature, pressure (from the hydrodynamic model resolution) and overall composition of the mixture, the value of the molar fraction of the solute in the expansion path (local equilibrium molar fraction, y_2) was calculated. As pointed out in the previous section, y_2 was calculated with the stability test.

In Figure 6 the supersaturation profile (S) for the three simulated conditions presented previously is shown. Naphthalene was extracted with carbon dioxide at 330 K and 150 bar, yielding an overall naphthalene molar fraction of 0.022. Thus, in Simulation 1 (T_0 = 330 K and P_0 = 150 bar) the system began the expansion already saturated (S = 1). In Simulation 2 (T_0 = 380 K and P_0 = 200 bar) the expansion began subsaturated (S<1), since the local equilibrium fraction was higher than the overall composition at the capillary inlet. It should be noted that in Simulation 2, the system was in a one-phase region, and no stable roots in the SF or VL equilibrium were present at the capillary inlet. In Simulation 3 (T_0 = 340 K and P_0 = 280 bar), the system also began expansion under a subsaturated condition (S < 1).

In Figure 6 it can be observed that supersaturation values are very high in the free-jet expansion region. On the other hand, depending on the preexpansion conditions, the supersaturation profile in the free jet region is quite different. These observations suggest that pre and post expansion conditions can have a remarkable effect on the characteristics of precipitated particles. It should be called that the preexpansion conditions also affect the profile for the expansion variables.

A discontinuous region in the supersaturation curves can also be seen in Figure 6. This fact is due to the absence of stable roots in the stability test. In these regions, the solute molar fraction calculated with equation 8 is very low (typically lower than $1.0x10^{-8}$). Calculating tR values for the RESS process (Figure 3), it can be concluded that under the initial subsaturated or saturated condition the solution moves very fast to a very high supersaturated condition. This observation shows the strong driving force for formation of a new solid phase formation in the RESS process.

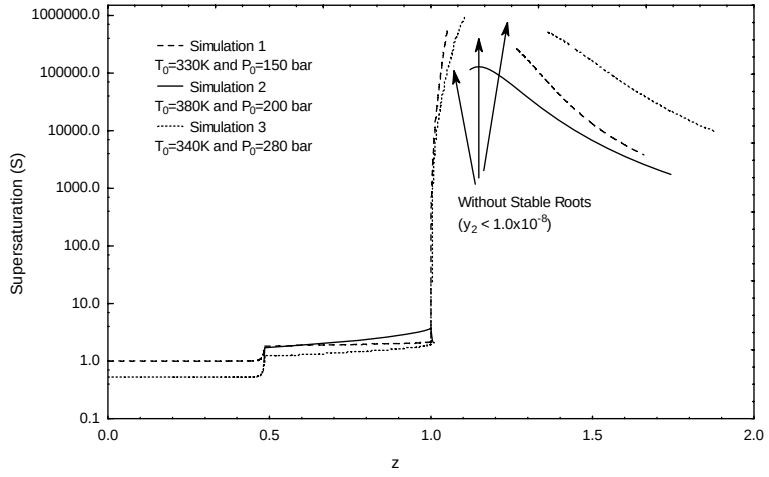

Figure 6: Supersaturation profile during expansion for the carbon dioxide(1)+naphthalene(2) system.

In order to evaluate the effect of solvent, a simulation of the propane(1)+naphthalene(2) system was conducted. The extraction conditions of 50 bar and 305 K (y_E = 0.059) were selected, while the preexpansion temperature and pressure were T_0 = 410 K and P_0 = 100 bar, respectively. All other simulation conditions were the same as those employed for carbon dioxide. Binary interaction parameters were taken from Corazza et al. (2004b). Figure 7 contains the supersaturation profile for the propane(1)+naphthalene(2) system.

In Figure 7 it can be observed that the calculated supersaturation values (around 10^4) are much lower than those observed for the carbon dioxide(1)+naphthalene(2) system, as the solubility of naphthalene in propane is higher than it is in carbon dioxide. Thus, the formation of a stable solid phase takes place in the free jet region, not occurring

inside the capillary (under the simulation conditions, the one-phase system is a stable condition inside the capillary).

It is important to mention that the size of the precipitated particles is affected by the supersaturation rates in the flow. In general, higher supersaturations result in lower particle size. Thus, the use of propane can produce larger particles than precipitation in a carbon dioxide medium. On the other hand, the very low solubility of solids in carbon dioxide makes the process unattractive, since a very small amount of material is processed. A solvent mixture composed of carbon dioxide and propane could be an alternative, since more material could be processed with high supersaturation rates in the RESS process.

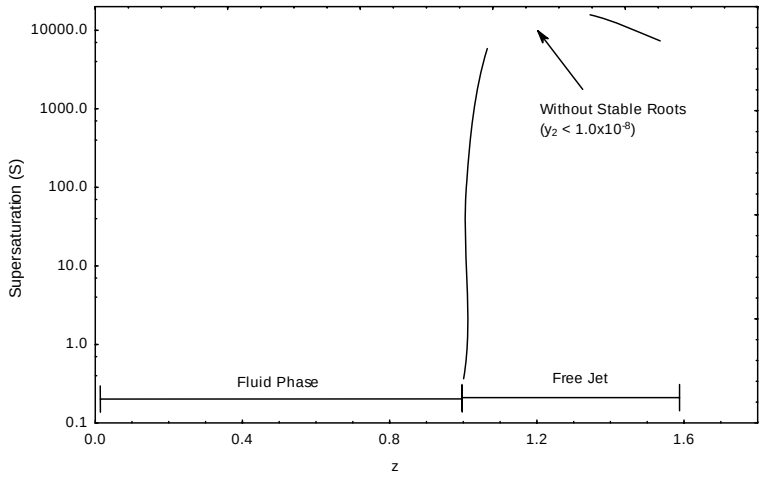

Figure 7: Supersaturation profile during expansion for the propane(1)+naphthalene(2) system.

CONCLUSIONS

The results presented in this work indicate that the fluid residence time in the capillary region is very low, around $1.0x10^{-4}$ s, and thus the mechanism for microparticle formation could also be affected by mass transfer phenomena in addition to thermodynamic equilibrium. The stability test coupled with a hydrodynamic simulation of the RESS process is an important tool for identifying the location of particle precipitation in the expansion path in the RESS process.

NOMECLATURE

Symbols

A	flow cross-sectional area	(m^2)
D_N	capillary diameter	(m)
D_M	diameter of free jet region	(m)
$\dot{m}$	mass flow	(kg/s)
L	section length	(m)
Ma	Mach number	(local velocity / speed of sound)
N	components number in the mixture	(bar)
P	pressure	(-)
q	heat flux	(kJ/kg)
R	constant of ideal gases	(8.314 bar.cm^3/(mol.K))
S	supersaturation rate	
tR	residence time	(s)
v	flow velocity	(m/s)
$\overline{v}$	mean velocity	(m/s)
x	axial position	(m)
y	molar composition in fluid phase	(-)
z	dimensionless length	(-)

Greeks Letters

$\hat{\phi}$	fugacity coefficient of fluid phase	(-)
f	fugacity of pure component	(bar)
$\hat{f}$	fugacity in fluid phase	(bar)
f	Fanning friction factor	(-)
ρ_M	density	(kg/m^3)
h	heat transfer coefficient	(1.10^7 W/(m^2.K))

Subscripts

I	inlet capillary section	(-)
II	constant area section (capillary)	(-)

III	free jet section	(-)
0	initial condition of flow	(initial value)
i	index of component in mixture	(-)
k	index of DAE solution	(-)
C	critical properties	(-)
E	extraction condition	(-)
ch	expansion chamber condition	(-)

Superscripts

fus	fusion condition	(-)
S	solid state	(-)
Sat	saturation condition	(-)
F	fluid state	(-)
UCEP	up critical end point	(-)
0	tested phase	(-)

REFERENCES

Arai, Y., Sako, T., and Takebayashi, Y., Supercritical Fluids: Molecular Interactions, Physical Properties, and New Applications, Springer, Germany (2002).

Baker, L.E., Pierce, A.C., and Luks, K.D., Soc. Petrol. Engrs. J., 22, 731 (1982).

Beckman, E.J., Supercritical and Near-critical CO_2 in Green Chemical Synthesis and Processing, J. Suppercritical Fluids, 28, 121-191 (2004).

Corazza, M.L., Cardozo-Filho, L., and Dariva, C., A Robust Strategy for SVL Equilibrium Calculations at High Pressures, Fluid Phase Equilibria, 221, 113 (2004a).

Corazza, M.L., Cardozo-Filho, L., and Dariva, C., SLV Equilibrium for CO_2+Co-Solvent+Solute System: Experimental Data And Modeling. CD-ROM. V EBFS, Florianópolis, SC, Brazil, April (2004b).

Diefenbacher, A., Türk, M. Phase Equilibria of Organic Solid Solutes and Supercritical Fluids with Respect to the RESS Process, J. Supercritical Fluids, 22, 175 (2002).

Domingo, C., Wubbolts, F.E., Rodriguez-Clemente, R., and Van Rosmalen, G.M., Solid Crystallization by Rapid Expansion of Supercritical Ternary Mixtures. J. Crystal Growth, 198/199, 760 (1999).

Ehrig, R., Nowak, U., Oeverdieck, L., Deuflhard, P., Advanced Extrapolation Methods for Large Scale Differential Algebric Problems. In: High Performance Scientific and Engineering Computing, H.-J. Bungartz, F. Durst, and Chr. Zenger (eds.), Lecture Notes in Computational Science and Enginnering, Springer, 8, 233 (1999).

Helfgen, B., Türk, M., and Schaber, K., Theoretical and Experimental Investigation of the Micronization of Organic Solids by Rapid Expansion of Supercritical Solutions, Powder Technology, 110, 22 (2000).

Helfgen, B., Hils, P., Holzknecht, C., Türk, M., and Schaber, K., Simulation of Particle Formation During the Rapid Expansion of Supercritical Solutions, Aerosol Science, 32, 295 (2001).

Helfgen, B., Türk, M., and Schaber, K., Hydrodynamic and Aerosol Modeling of the Rapid Expansion of Supercritical Solutions (RESS-Process), J. Supercritical Fluids, 00, 1 (2002).

Hua, J.Z., Maier, R.W., Tessier, S.R., Brennecke, J.F. and Stadtherr, M.A., Interval Analysis for Thermodynamic Calcultations in Process Design: A Novel and Completely Reliable Approach: 8th International Conference on Properties and Phase Equilibria for Product and Process Design. Noordwijkerhout. Netherlands, April 26- May 1 (1998).

Jung, J. and Perrut, M., Particle Design using Supercritical Fluids: Literature and Patent Survey, J. Supercritical Fluids, 20, 179 (2001).

Ksibi, H. and Subra, P., Influence of Nozzle Design on the Nucleation Conditions in the Ress Process. I Fluidi Supercritici e Le Loro Applicatione. Ed: Kikic, I and Alessi, P. Grignano, Triete, Italy (1995).

Lele, A.K. and Shine, A.D., Morphology of Polymers Precipitated from a Supercritical Solvent, AIChE J., 38, 742 (1992).

Mcdonald, C. and Floudas, C.A., Global Optimization for the Phase Stability Problem, AICHE J., 41, 1798 (1995).

Michelsen, M. The Isothermal Flash Problem. Part I. Stability, Fluid Phase Equilibria, 9, 1 (1982).

Platzer, B. and Maurer, G., Application of a Generalized Bender Equation of State to Description of Vapor-Liquid Equilibria in Binary Systems, Fluid Phase Equilibria, 84, 79 (1993).

Press, W.H., Teukolsky, S.A., Vetterling, W.T., Flannery, B.P., Numerical Recipes in FORTRAN: The Art of Scientific Computing, Cambridge University Press, Second Edition (1992).

Reid, R.C., Prausnitz, J.M. and Poling, B.E., The Properties of Gases & Liquids. McGraw-Hill, Fourth Edition (1988).

Reverchon, E. and Pallado, P., Hydrodynamic Modelling of the RESS Process, J. Suppercritical Fluids, 9, 216 (1996).

Ribeiro dos Santos, I. Richard, J., Pecha, B., Thies, C. and Benoit, J.P., Microencapsulation of Protein Particles within Lipids using a Novel Supercritical Fluid Process, International Journal of Pharmaceutics, 21, 69 (2002).

Türk, M., Formation of Small Organic Particles by RESS: Experimental and Theoretical Investigations, J. Supercritical Fluids, 15, 79 (1999).

Türk, M., Hils, P., Helfgen, B., Schaber, K., Martin, H.-J. and Wahl, M.A., Micronization of Pharmaceutical Substances by Rapid Expansion of Supercritical Solutions (RESS): a Promising Method to Improve Bioavailability of Poorly Soluble Pharmaceutical Agents, J. Supercritical Fluids, 22, 75 (2002).

Weber, M., Russell, L.M. and Debenedetti, P.G., Mathematical Modeling of Nucleation and Growth of Particles Formed by the Rapid Expansion of a Supercritical Solution Under Subsonic Conditions. J. Supercritical Fluids, 23, 65 (2002).